



Understanding high wintertime ozone pollution events in an oil and natural gas producing region

R. Ahmadov et al.

Understanding high wintertime ozone pollution events in an oil and natural gas producing region of the western US

R. Ahmadov^{1,2}, S. McKeen^{1,2}, M. Trainer², R. Banta², A. Brewer², S. Brown², P. M. Edwards^{1,2,*}, J. A. de Gouw^{1,2}, G. J. Frost^{1,2}, J. Gilman^{1,2}, D. Helmig³, B. Johnson², A. Karion^{1,2}, A. Koss^{1,2}, A. Langford², B. Lerner^{1,2}, J. Olson^{1,2}, S. Oltmans^{1,2}, J. Peischl^{1,2}, G. Pétron^{1,2}, Y. Pichugina^{1,2}, J. M. Roberts², T. Ryerson², R. Schnell², C. Senff^{1,2}, C. Sweeney^{1,2}, C. Thompson³, P. Veres^{1,2}, C. Warneke^{1,2}, R. Wild^{1,2}, E. J. Williams², B. Yuan^{1,2}, and R. Zamora²

¹Cooperative Institute for Research in Environmental Sciences, University of Colorado at Boulder, Boulder, CO, USA

²Earth System Research Laboratory, National Oceanic and Atmospheric Administration, Boulder, CO, USA

³Institute for Arctic and Alpine Research, University of Colorado at Boulder, Boulder, CO, USA
* now at: Department of Chemistry, University of York, York, UK

Title Page

Abstract

Introduction

Conclusions

References

Tables

Figures



Back

Close

Full Screen / Esc

Printer-friendly Version

Interactive Discussion



Received: 15 July 2014 – Accepted: 18 July 2014 – Published: 8 August 2014

Correspondence to: R. Ahmadov (ravan.ahmadov@noaa.gov)

Published by Copernicus Publications on behalf of the European Geosciences Union.

ACPD

14, 20295–20343, 2014

Understanding high wintertime ozone pollution events in an oil and natural gas producing region

R. Ahmadov et al.

Title Page

Abstract

Introduction

Conclusions

References

Tables

Figures



Back

Close

Full Screen / Esc

Printer-friendly Version

Interactive Discussion

Abstract

Recent increases in oil and natural gas (NG) production throughout the western US have come with scientific and public interest in emission rates, air quality and climate impacts related to this industry. This study uses a regional scale air quality model WRF-Chem to simulate high ozone (O_3) episodes during the winter of 2013 over the Uinta Basin (UB) in northeastern Utah, which is densely populated by thousands of oil and NG wells. The high resolution meteorological simulations are able to qualitatively reproduce the wintertime cold pool conditions that occurred in 2013, allowing the model to reproduce the observed multi-day buildup of atmospheric pollutants and accompanying rapid photochemical ozone formation in the UB.

Two different emission scenarios for the oil and NG sector were employed in this study. The first emission scenario (bottom-up) was based on the US EPA National Emission Inventory (NEI) (2011, version 1) for the oil and NG sector for the UB. The second emission scenario (top-down) was based on the previously derived estimates of methane (CH_4) emissions and a regression analysis for multiple species relative to CH_4 concentration measurements in the UB. WRF-Chem simulations using the two emission data sets resulted in significant differences for concentrations of most gas-phase species. Evaluation of the model results shows greater underestimates of CH_4 and other volatile organic compounds (VOCs) in the simulation with the NEI-2011 inventory than the case when the top-down emission scenario was used. Unlike VOCs, the NEI-2011 inventory significantly overestimates the emissions of nitrogen oxides (NO_x), while the top-down emission scenario results in a moderate negative bias. Comparison of simulations using the two emission data sets reveals that the top-down case captures the high O_3 episodes. In contrast, the simulation case using the bottom-up inventory is not able to reproduce any of the observed high O_3 concentrations in the UB. A sensitivity analysis reveals that the major factors driving high wintertime O_3 in the UB are shallow boundary layers with light winds, high emissions of VOCs from oil and NG operations compared to NO_x emissions, enhancement of photolysis fluxes and reduc-

Understanding high wintertime ozone pollution events in an oil and natural gas producing region

R. Ahmadov et al.

Title Page

Abstract

Introduction

Conclusions

References

Tables

Figures

◀

▶

◀

▶

Back

Close

Full Screen / Esc

Printer-friendly Version

Interactive Discussion



Understanding high wintertime ozone pollution events in an oil and natural gas producing region

R. Ahmadov et al.

Title Page

Abstract

Introduction

Conclusions

References

Tables

Figures

◀

▶

◀

▶

Back

Close

Full Screen / Esc

Printer-friendly Version

Interactive Discussion

ment of the oil and NG industry over the last several years (Oltmans et al., 2014). The high O_3 episodes in both the UGRB and UB were associated with oil and NG production occurring in below freezing temperatures, industry emissions of O_3 precursors and when persistent snow cover is present under prevailing light wind conditions and associated clear skies. This combination produces strong, shallow temperature inversions that trap fossil fuel effluents in a stable boundary layer. Sunlight passing through the trapped gasses and reflecting back off the high albedo snow drives diurnal photochemical production of O_3 that peaks soon after solar noon in concentrations as high as 160 ppb (Schnell et al., 2009). In the absence of the above meteorological conditions, O_3 concentrations were near the background levels, in the 40–50 ppb range in the UGRB and UB (Oltmans et al., 2014).

It should be noted that the impact of the oil and NG production on ambient air quality goes beyond the wintertime. Kemball-Cook et al. (2010) modeled the impact of the Haynesville Shale development on ambient O_3 levels in Texas and Louisiana. Their photochemical modeling of the year 2012 showed increases in 8 h average ozone values of up to 5 ppb within northeast Texas and northwest Louisiana resulting from development in the Haynesville Shale. A model study by Rodriguez et al. (2009) found that the rise of oil and NG production in the Intermountain West could increase maximum 8 h average O_3 levels by 9.6 ppb in southwestern Colorado and northwestern New Mexico in summer. Cooper et al. (2012) analyzed long term surface O_3 measurements at rural sites from 1990–2010 across the US observing that eastern US sites exhibited a decrease in summertime O_3 over that period, while the western sites did not show a decrease in summertime O_3 . These findings imply importance of future research to accurately quantify the role of rising oil and NG emissions in the western US to the ambient O_3 levels.

Researchers from NOAA and other partnering organizations conducted intensive measurement field missions in the UB (Fig. 1) during the winters of 2012, 2013 and 2014. The full review of the Uinta Basin Winter Ozone Study (UBWOS) field campaign in 2013 can be found in the report available at: <http://www.deq.utah.gov/locations/U/>

uintahbasin/studies/UBOS-2013.htm. The topography of the UB is shown on Fig. 1. In this study we used the measurements from the 2012 and 2013 field campaigns only. The 2012 and 2013 wintertime meteorological and chemical conditions were sharply different. During January and February 2012 the UB experienced relatively warm weather (above freezing temperatures during daytime) and the ground was almost snow free, thus the meteorological conditions were not favorable for O₃ production. In contrast, during the winter of 2013 the ground was covered by a layer of snow (~ 20–30 cm) and air temperatures were typically 10–15 °C lower than in 2012. Consequently during UBWOS-2013, high O₃ episodes were frequently experienced. Helmig et al. (2014) analyzed observations of VOCs from both UBWOS 2012 and 2013 field campaigns. The study revealed that the concentrations of such air pollutants as benzene and toluene in the UB during winter of 2013 exceeded 5–10 times the reported values of those species over major US cities. While focusing on simulations for 2013, we also present results for 2012, using identical emission scenarios for both years for comparison.

During UBWOS-2013 the UB was mostly under the influence of synoptic scale surface high pressure systems. These conditions resulted in frequent stagnation events in the UB with light wind and shallow boundary layers. The stagnation episodes were discontinued by occasional storms passing over the UB. The snow cover prevented the heat exchange of air with the ground. Consequently, the boundary layers were shallow (~ 50–200 m) during daytime. Thus, persistent stagnant meteorological conditions were present throughout most part of the 2013 study period in the UB. During the UBWOS field campaigns a large variety of meteorological, chemistry, and flux measurements were conducted at the Horse Pool ground site (Fig. 1). In addition, frequent tethersonde balloon launchings took place at three sites during winter of 2013 producing high resolution vertical profiles of O₃, temperature, and humidity (Oltmans et al., 2014). These sites include Horse Pool, Ouray and Fantasy Canyon locations shown in Fig. 1 in the UB.

Understanding high wintertime ozone pollution events in an oil and natural gas producing region

R. Ahmadov et al.

Title Page

Abstract

Introduction

Conclusions

References

Tables

Figures

◀

▶

◀

▶

Back

Close

Full Screen / Esc

Printer-friendly Version

Interactive Discussion



Understanding high wintertime ozone pollution events in an oil and natural gas producing region

R. Ahmadov et al.

Title Page

Abstract

Introduction

Conclusions

References

Tables

Figures

◀

▶

◀

▶

Back

Close

Full Screen / Esc

Printer-friendly Version

Interactive Discussion

The high wintertime O₃ observations have motivated researchers to attempt to model the photochemical processes driving the O₃ production resulting from the oil and NG production related emissions. Carter and Seinfeld (2012) used a detailed chemical mechanism in a box model to study high O₃ production observed at two sites in the UGRB in 2008 and 2011. The authors performed multiple sensitivity analyses to assess the effects of ambient VOC speciation, air temperature and atmospheric radiation conditions on the O₃ production. The study found that one site for the 2008 episode was highly NO_x sensitive and insensitive to VOCs and nitrous acid (HNO₂), while the other 2008 case and both 2011 cases were highly sensitive to changes in specified VOC and HNO₂ concentrations. The authors stressed the need for full three dimensional (3-D) air quality models to address the high O₃ episodes in the UGRB and similar regions due to regional variability in photochemical and meteorological conditions.

Edwards et al. (2013) conducted a box modeling study of O₃ production in the UB in winter 2012 using a near-explicit gas chemistry scheme – Master Chemical Mechanism v3.2 for data collected at the Horse Pool site during the UBWOS-2012 field campaign. According to their box modeling study, the photochemical regime during that period was characterized as radical limited. Edwards et al. (2014) used a similar chemical box model for the conditions observed in winter of 2013 in the UB. The study concluded the importance of the build-up and photolysis of carbonyls in deriving high O₃ in the UB during winter of 2013.

The stagnant meteorological conditions during the winter of 2013 in the UB are characterized as a “cold pool”. Cold pool type inversion layers occurring within basins and valleys in the western US have been extensively studied (Banta and Cotton, 1981; Clements et al., 2003; Lareau et al., 2013). Such valley cold pools (VCP) are identified when a radiosonde indicates the presence of an inversion below the maximum crest height of the surrounding mountains and average wind speeds beneath the inversion top that are less than 5 m s⁻¹ (Reeves and Stensrud, 2009). The VCPs are caused by an approaching upper-level trough and midlevel cooling and they can exist several days until being removed usually by advection or turbulent erosion processes (Reeves

Understanding high wintertime ozone pollution events in an oil and natural gas producing region

R. Ahmadov et al.

Title Page

Abstract

Introduction

Conclusions

References

Tables

Figures

◀

▶

◀

▶

Back

Close

Full Screen / Esc

Printer-friendly Version

Interactive Discussion

et al. (2013). Point source emission estimates within the top-down scenario are also based on the NEI-2005, while the bottom-up point sources emission estimates are specified according to the NEI-2011 national inventory. Since the NEI-2005 inventory does not include any oil/gas sector emissions for the UB, double counting of emissions in the top-down emission data set is avoided by using NEI-2005 for non oil/gas sector emission estimates.

The coal fired Bonanza power plant (Fig. 1) located in the southeastern part of the UB is the predominant point source of NO_x and sulfur dioxide (SO_2) in the UB. Measurements during the winter 2013 study showed that when shallow boundary layers were present, the power plant effluents were injected into the free atmosphere. For the UB domain used here, CH_4 and VOC emissions are dominated by the oil and gas production sector within the area (or nonpoint) source category. Details of the emissions processing for this sector and for the two emission data sets are presented below. Due to the geographical location of the UB (Fig. 1), and locations of the emission sources in the vicinity, the upwind transport of air pollution to the UB is small. The major pollution source outside of the basin is Salt Lake City, which is located more than 100 km away. It should be noted that the UB is sparsely populated, thus the urban emissions are small.

2.1 EPA NEI-2011 oil/gas sector emissions (bottom-up)

The bottom-up emission inventory for the UB oil/gas sources is based on the US EPA NEI-2011 (version 1) national inventory released in August 2013 (US EPA, 2013, available at ftp://ftp.epa.gov/EmisInventory/2011v6/flat_files). The national inventory contains annual emission estimates of total VOCs from the oil/gas sector at a county level for nonpoint sources, or at specific locations for point sources. Ancillary information for temporal partitioning, VOC speciation, and spatial distribution of nonpoint sources are available through data files in the version 1 modeling platform (<ftp://ftp.epa.gov/EmisInventory/2011v6/v1platform>, release date 11 August 2013). The EPA SPECIATE 4.3 database (e.g. Simon et al., 2010) is used for default VOC profile species assignments and the VOC to total organic gases (including CH_4) emission conversions. Within

Understanding high wintertime ozone pollution events in an oil and natural gas producing region

R. Ahmadov et al.

Title Page

Abstract

Introduction

Conclusions

References

Tables

Figures

◀

▶

◀

▶

Back

Close

Full Screen / Esc

Printer-friendly Version

Interactive Discussion



the modeling platform, the oil/gas sector VOC speciation for nine distinct oil and natural gas producing basins are specified according to Western Regional Air Partnership recommendations (http://www.wrapair.org/forums/ogwg/PhaseIII_Inventory.html). Four distinct VOC speciation profiles are provided for the UB, and mapped with EPA assignments (gsref_cmaq_cb05_soa_2011ec_v6_11f_onroad_06sep2013.txt), to the source classification code, or activity, that is provided with the state-supplied VOC emission estimates. VOC profile to VOC species assignments are available for the Carbon Bond version 5 (CB-05) chemical mechanism within the file gspro_cmaq_cb05_soa_2011ec_v6_11f_beis_nf.txt. CB-05 VOC speciation assignments to the Regional Atmospheric Chemistry Mechanism (RACM) (Stockwell et al., 1997) chemical mechanism is straightforward for non-alkane species (mostly formaldehyde, toluene, xylenes and ethylene). The weight fraction of “PAR”, representing the lumped alkane class within CB-05, was partitioned into the RACM alkane classes according to the alkane partitioning observed at the Horse Pool site during 2012 and 2013. We refer to this emission inventory as “bottom-up” further in the text.

Primary NO_x emissions are specified as 90 % nitric oxide (NO), 8 % nitrogen dioxide (NO_2) and 2 % HNO_2 that are ratios used within the California Air Resources Board non-point sources (http://orthus.arb.ca.gov/calnex/data/discl_calnex2010.html). This partitioning was applied to both bottom-up and top-down emission data sets, though model results are shown to be insensitive to this partitioning in Sect. 4.2.3 below. The hourly emissions of the gaseous species were added to the chemical species mixing ratios in the model at every time step during the model integration using temporal profile assignments from cross-reference files in the NEI-2011 version 1 model platform database. The CH_4 emissions were indirectly determined from total VOC estimates within NEI-2011, and the total organic gas to reactive organic gas ratios specified within the SPECIATE 4.3 software.

2.2 Top-down oil/gas sector emission estimates

The top-down oil/gas emission estimates for the UB region are based on regression slopes of NO_y and 59 individual VOCs with CH₄ observed during daylight hours at the Horse Pool site during the winters of 2012 and 2013. Regressions are determined for observations taken between 10:00–16:00 Mountain Standard Time (MST) for two reasons: (1) a broader, more regional representative sample is available during daylight hours when the boundary layer is active, (2) large transient spikes in NO_y, VOC and CH₄ observed mostly during stable nighttime conditions that can decrease correlations and influence regression slopes are removed. Absolute emission values are specified by scaling regression slopes with the Uintah County (located in the eastern part of the UB) mean CH₄ flux estimate of $55 \times 10^3 \text{ kg CH}_4 \text{ h}^{-1}$ as determined from upwind and downwind aircraft transects during one flight in February 2012 (Karion et al., 2013). We distribute this estimated emission over the entire UB, which includes both Uintah and Duchesne (located in the western part of the UB) counties, even though the aircraft measurement used by Karion et al. (2013) covered only the eastern part of the UB. We used this estimate, as it is the only available top-down estimate of CH₄ flux for the oil/gas sector in the UB at present. Here we assume this emission estimate is representative for 2013 as well. A summary of the regression slopes, r^2 Pearson correlation coefficients, and partitioning within the photochemical mechanism is presented in the supplemental information (SI) Table S1. It should be noted that the VOC to CH₄ ratios reported here agree quite well with the independent estimates carried out by Helmig et al. (2014).

No hourly variation is assumed in the top-down emission scenario for the oil/gas sector. Here the oil/gas emissions are spatially allocated according to well numbers in a given model grid cell, using well location information from the Department of Oil, Gas and Mining, Utah Department of Natural Resources (http://oilgas.ogm.utah.gov/Maps/OG_Maps.htm), valid as of May 2012. VOC speciation is assumed the same for both oil and NG wells. Only wells within Duchesne and Uintah counties are considered.

Understanding high wintertime ozone pollution events in an oil and natural gas producing region

R. Ahmadov et al.

Title Page

Abstract

Introduction

Conclusions

References

Tables

Figures

◀

▶

◀

▶

Back

Close

Full Screen / Esc

Printer-friendly Version

Interactive Discussion

Understanding high wintertime ozone pollution events in an oil and natural gas producing region

R. Ahmadov et al.

Title Page

Abstract

Introduction

Conclusions

References

Tables

Figures

◀

▶

◀

▶

Back

Close

Full Screen / Esc

Printer-friendly Version

Interactive Discussion



Here the spatial pattern of NO_x , VOCs, and CH_4 emissions from oil and NG operations in both counties are assumed to depend only on well density as a simple first-order approximation. Additional information would be needed to more accurately locate significant isolated emission sources associated with combustion and fugitive processes within the UB. These sources include, but are not limited to, evaporation ponds, diesel generators used in the oil and NG well drilling, oil storage tanks, compressors, NG compressor stations, processing plants and venting operations. We name this emission set as “top-down”, because it relies on the atmospheric measurements made by an aircraft (Karion et al., 2013) and at the surface site.

Figure 2a and b show the spatial distribution of 24 h averaged total toluene emissions over the UB in the 4 km resolution model grid from both emissions sets, with the emissions in Fig. 2b being proportional to the spatial density of the oil and NG wells. There are two high emission spots in the region, one in the western part of the UB, another to the east, south of Horse Pool.

Total fluxes of CH_4 , VOCs and NO_x from both emission scenarios for the oil/gas and other sectors in the UB are provided in Table 2. CH_4 and total VOC emissions for the oil/gas sector within the UB in the bottom-up inventory (NEI-2011) are lower by a factor of 4.8 and 1.8 than the top-down estimates, respectively. Conversely, NO_x emissions are about 4 times higher in the bottom-up inventory. The large difference in VOC/ NO_x emission ratios between the two products is shown below to have a profound impact on modeled O_3 formation within the UB. Table 2 also shows that VOC emissions from the oil/gas sector dominate emissions from all other sources (vehicle, residential etc.) in the UB, and that NO_x emissions are dominated by the oil/gas sector in the bottom-up inventory but not in the top-down emission data set. We assumed NO_y as an inert species in deriving the NO_x emissions.

3 Air quality model description

The WRF-Chem model is a fully coupled meteorology-chemistry model (Grell et al., 2005), and a recent version of the model (version 3.5.1) was used in this study (<http://ruc.noaa.gov/wrf/WG11/>). The main WRF-Chem model settings are presented in Table S2. The gas phase chemistry mechanism used here is called “RACM_ESRL” within the WRF-Chem model. The RACM_ESRL gas chemistry scheme is based on the RACM mechanism (Stockwell et al., 1997), which is designed to be suitable for modeling full tropospheric chemistry in remote and polluted regions. The RACM_ESRL mechanism contains additional chemical reactions, species and updated rate coefficients as discussed within Kim et al. (2009). The mechanism contains a wide range of inorganic and organic species and their intermediates, which are advected and vertically mixed at every time step during model integration, and includes 16 photolysis and 221 chemical reactions. It has been successfully used in previous air quality model studies, e.g. Kim et al. (2009, 2011), Ahmadov et al. (2012). The advantage of the WRF-Chem model is that the same 3-D model grid, time step and advection scheme are used for both meteorological and chemical variables. Below we describe some specifications and modifications to the WRF-Chem 3.5.1 code that are needed for the wintertime UB simulations of 2012 and 2013.

The dry deposition of gas species is parameterized following Erisman et al. (1994). As the default WRF-Chem code was intended to simulate summertime O₃, the deposition scheme uses “snow or ice” type of land use category solely for the areas permanently covered by ice, e.g. the Arctic. The deposition scheme was modified to treat model grid cells as “snow or ice” whenever they are covered by snow. This helps to properly simulate dry deposition fluxes of O₃ and other species to the snow-covered ground for the 2013 simulations.

We used the Tropospheric Ultraviolet and Visible (TUV) photolysis scheme (Madronich, 1987) within WRF-Chem. The column density for O₃ in the photolysis scheme was set to 270 Dobson unit (DU) based on the OMI satellite data set

Understanding high wintertime ozone pollution events in an oil and natural gas producing region

R. Ahmadov et al.

Title Page

Abstract

Introduction

Conclusions

References

Tables

Figures

◀

▶

◀

▶

Back

Close

Full Screen / Esc

Printer-friendly Version

Interactive Discussion

(<http://mirador.gsfc.nasa.gov/>) for the simulation time period (February 2013) and latitude. Additionally, the photolysis scheme was modified to include the effect of snow on surface albedo. The snow effect on photolysis is not considered in the default WRF-Chem model developed primarily for summertime photochemistry, similar to other air quality models. Based on the measured albedo values during the UBWOS field campaign in 2013, a fixed value of 0.85 was set for the surface albedo in the photolysis module when a given grid cell was covered by snow. The default values of the surface albedo appropriate for bare ground conditions in the TUV scheme lies within the range of 0.05–0.15 depending on the wavelength.

North American Mesoscale analysis fields (www.emc.ncep.noaa.gov) were used as boundary and initial conditions for the meteorological fields. Idealized vertical profiles were used as initial and boundary conditions to assign the background mixing ratios for some of the long lived chemical species.

The meteorology and chemistry were simultaneously simulated by the WRF-Chem model initially on the 12 km resolution domain, covering a large part of the western US. For this domain the bottom-up anthropogenic emissions inventory was used in the simulations. Model simulations were conducted using the same settings and emissions for both January–February 2012 and 2013 time periods. The second stage of WRF-Chem simulations were conducted on a 4 km resolution domain by performing one-way downward nesting from the 12 km domain simulations whereby the output from the coarse domain simulations was used to provide initial and boundary conditions for the meteorological and chemical variables (mixing ratios of the gas species) in the 4 km model domain. Hereafter we present the modeling results solely from simulations done on the 4 km model grid, as this domain can better represent the “cold pool” conditions and the complex topography in the region.

4 Discussion of results

4.1 Base case simulations

First, we present O₃ modeling results for UBWOS-2012. Figure 3a shows time series of measured and modeled O₃ concentrations during 31 January–28 February 2012 at the Horse Pool site. There are three modeling cases here, which were performed in the same way, except for different emission scenarios – bottom-up, top-down, and top-down without any oil/gas emissions in the UB. Observed hourly O₃ mixing ratios at the site reach ~ 40 ppb during afternoon hours, while the variability of daytime O₃ from one day to another is small, and none of the emission cases differ markedly. The variability of O₃ within the UB is dominated by transport of background O₃ into the Basin rather than by local chemistry. As noted before, the meteorological conditions did not result in any O₃ exceedances during the 2012 field campaign. Maximum O₃ values during daytime are reasonably well simulated by both cases, while the bottom-up inventory shows stronger O₃ depletion due to NO_x titration during nighttime. The model case without the oil/gas emissions is slightly different than the top-down case, indicating a small contribution of the oil/gas sector to O₃ production in the UB for 2012.

Figure 3b demonstrates measured and modeled time series of O₃ at Horse Pool for 29 January–21 February 2013. The sharp contrast in hourly O₃ concentrations between the two years is clear. Daytime O₃ concentrations on most days exceeded by 2–3 times the O₃ concentrations observed in 2012. Unlike the 2012 time period, model results with the three emission scenarios for 2013 differ considerably. The simulation using the bottom-up emission set cannot capture any of the O₃ enhancements observed at Horse Pool in 2013. However, the modeling case using the top-down emissions is able to simulate the high O₃ episodes, the multiday buildup of O₃ in the UB, and the removal of O₃ from the UB due to meteorological forcing between each high O₃ episode. When all the oil/gas emissions are removed from the top-down inventory, model O₃ is very close to the background mixing ratios of ~ 40 ppb, indicating a significant contribution of the local oil/gas emissions to high O₃ production in the UB in winter

of 2013. The low model bias of O₃ during nighttime at Horse Pool is caused by stronger katabatic winds in the model, which advect cleaner background air from outside the UB to Horse Pool at night within a very shallow layers above the surface. Further we refer to the model simulation for 2013 using the top-down emission scenario as “base case”.

Statistical evaluations of O₃ and other gas-phase species measured at Horse Pool and simulated with the first two emission scenarios and for both 2012 and 2013 are provided in Table 3a and b. Hereafter, we report the model evaluation statistics for daytime measurements only, between 09:00–17:00 MST, since the atmospheric models have difficulties in accurately simulating stable nocturnal planetary boundary layers (PBL), when the PBL depth could be a few meters. These tables also provide the median of observed values for several chemical species at Horse Pool during the 2012 and 2013 field campaigns. The detection methods used to obtain these measurements are described in detail by Warneke et al. (2014). The median of the measured mixing ratios of primary and secondary chemical species highlight the contrast in pollutant levels in the UB between the two consecutive years.

The evaluation statistics reveal that the model captures the temporal variability of primary species better in 2012 than in 2013. This could be caused by the fact that during 2013 turbulent mixing and advection were much weaker than in 2012, and uncertainties in the spatial representation of emissions would affect the correlations for primary species more strongly in the 2013 evaluations. This would likely be the case for both bottom-up and top-down emission cases. Primary species such as NO_y and some non-methane hydrocarbons are somewhat underestimated during daytime for the top-down emission case in both 2012 and 2013. Table 3a clearly demonstrates that the bottom-up inventory leads to a stronger model underestimation of CH₄ in 2012 compared to the top-down emission estimates. The evaluation of CH₄ simulations at a ground site provides an independent validation of the CH₄ flux estimates from the oil and NG operations in the UB determined by using aircraft measurements. The discrepancy between the emission scenarios in terms of CH₄ simulations widens in 2013 simulations (Table 3b), when high CH₄ levels were observed at Horse Pool. However

Understanding high wintertime ozone pollution events in an oil and natural gas producing region

R. Ahmadov et al.

Title Page

Abstract

Introduction

Conclusions

References

Tables

Figures

◀

▶

◀

▶

Back

Close

Full Screen / Esc

Printer-friendly Version

Interactive Discussion

Understanding high wintertime ozone pollution events in an oil and natural gas producing region

R. Ahmadov et al.

Title Page

Abstract

Introduction

Conclusions

References

Tables

Figures

◀

▶

◀

▶

Back

Close

Full Screen / Esc

Printer-friendly Version

Interactive Discussion

the top-down emission case still underestimates CH₄ levels by ~ 40%. This model underestimation may be caused by two sources of error that could potentially offset each other. First, as stated above the CH₄ flux estimate of Karion et al. (2013) used to scale the primary emissions is likely a lower limit, since the estimate is limited to a single day of aircraft sampling that only sampled emissions from the oil and NG operations emissions in the eastern part of the UB. Second, biases in the model meteorological fields, such as wind speed, and mixing layer height could be affecting either year's statistics.

Evaluation of the model for other gaseous species at Horse Pool for the two emission cases reveals that the bottom-up emissions (NEI-2011) lead the model to strongly overestimate the NO_y concentrations, while the VOCs are greatly underestimated (Table 3a and b). Using the top-down emission scenario the model explains the temporal variability in the primary species such as NO_y, alkanes (ethane), and aromatics (toluene and xylene) better than the bottom-up inventory in 2013, while the two cases are not that different in 2012. This shows the advantage of the top-down emission estimates compared with the bottom-up (NEI-2011) case for the oil/gas emissions in the UB. The model captures both the temporal variability and daytime values of secondary species such as O₃, peroxyacyl nitrates (PAN) and acetaldehyde (CH₃CHO) in 2013 quite well.

Table 3a reveals that for 2012 both emissions cases show very similar correlations for the daytime O₃ concentrations, as the O₃ concentrations were slightly affected by local emissions and photochemistry. However, in 2013 the top-down emission case exhibits profoundly better correlation than the bottom-up case. The top-down emission case captures both the magnitude and variance of the daytime O₃ values at Horse Pool well. In Table 3a and b the statistics for odd oxygen (O_x = O₃ + NO₂) are also shown. This helps to identify the role of O₃ titrated by freshly emitted NO_x in the model and observation. The bias statistics show that the top-down emission scenario allows the model to capture the secondary species, which are products of the photochemistry. Conversely, the bottom-up inventory results in strong underestimation of the secondary species during 2013.

Understanding high wintertime ozone pollution events in an oil and natural gas producing region

R. Ahmadov et al.

Title Page

Abstract

Introduction

Conclusions

References

Tables

Figures

◀

▶

◀

▶

Back

Close

Full Screen / Esc

Printer-friendly Version

Interactive Discussion

The statistical comparisons in Table 3a and b for reactive nitrogen species show a marked difference between 2012 and 2013 for the top-down emission case. Both years show a 25 to 30 % low bias in NO_y . One would expect biases in individual NO_y species to reflect the bias of NO_y itself, which is the case for NO_x , nitric acid (HNO_3), and PAN in 2012. But in 2013 NO_x shows a positive bias, and HNO_3 is significantly under predicted relative to NO_y . The HNO_3 underprediction can be explained by high HNO_3 deposition velocities in the default version of the WRF-Chem model used here. Measurements of HNO_3 deposition to snow indicate a very low deposition velocity at cold temperatures (Johansson and Granat, 1986), and even HNO_3 emissions from snow due to heterogeneous conversion of other reactive nitrogen species to nitrate at the snow surface (Dibb et al., 1998). The overprediction of NO_x may likewise be related to uncertainties in the deposition of NO_2 to the snow-covered surface, but as discussed further below in the model sensitivity section, nighttime heterogeneous conversion of N_2O_5 to aerosol, which is not included in our base model configuration, could explain part of the NO_x discrepancy during 2013.

In order to demonstrate how well the model parameterizes the photochemistry in both emission cases, we plot measured and modeled O_x vs. PAN during the daytime for 2013 (Fig. 4). As seen from the scatter plot, the base case (top-down emission scenario) is able to predict the observed relationship between O_x and PAN. The model case with the bottom-up inventory also matches the observed O_x -PAN relationship, but over a much smaller concentration range. As only the top-down emission inventory can explain the high O_3 in the UB in 2013, we analyze this base case model scenario in more detail below.

The time period shown on Fig. 3b consists of three distinct episodes with high O_3 measurements. We group these episodes as follows: the first and longest episode covers the 29 January–8 February time period. The other two episodes cover 12–17 February and 19–21 February 2013. Between the episodes, synoptic scale surface low pressure systems were present which led to the partial clearing of O_3 and other pollutants out of the UB. Such meteorological conditions occurred prior to 29 January

and between the stagnation episodes. Weather maps in Fig. S1 show synoptic situations associated with a frontal passage and stagnation episode occurred in the UB during UBWOS-2013. Hereafter, we focus on the 29 January to 8 February stagnation period. Meteorological conditions associated with O₃ buildup for other time periods are very similar to this episode. We also provide evaluations for some of the meteorological variables over the same time period in the SI.

Figure 5a and b illustrates the simulated O₃ distribution within the UB during a high ozone event. Modeled O₃ mixing ratios and horizontal wind vectors over the vertical plane across the Ouray and Horse Pool sites (Fig. 1) are shown at night (05:00 MST) and in the afternoon (15:00 MST) on 5 February 2013, a typical stagnation day when O₃ levels reached their February maximum at Horse Pool (Fig. 3b). The plots show the very low wind speed inside the UB, demonstrating the wind regime during a VCP type situation. Figure 5a shows the high O₃ in early morning above the western slope. The highest O₃ mixing ratio is simulated at ~ 100 m above ground at night. The downslope terrain flows converge at the bottom of the UB. Later the layer enriched with O₃ and other pollutants aloft, is moved to the eastern part of the UB during the morning hours. As we show in the SI, the wind speed of the nocturnal drainage flows over the UB are overestimated at Horse Pool and possibly elsewhere. This overestimation likely causes a stronger and faster drainage and updraft of the air masses near the ground at night, than what was observed. Then, the shallow vertical mixing layer that developed along the slopes of the UB dilutes the pollutants aloft within itself. The afternoon O₃ distribution for the same vertical plane shows the horizontal and vertical extent of the O₃ buildup in the UB (Fig. 5b). O₃ mixing ratios reached ~ 120 ppb over Horse Pool and Ouray at 15:00 MST. The highest O₃ buildup is simulated between these two sites. The mixed layer with high O₃ (> 100 ppb) is ~ 100 m thick during the daytime. High O₃ buildup (~ 100 ppb) is simulated over the western part of the UB, reaching as high as 1900 m a.s.l. on the western slope. Another prominent feature on this particular day in the vertical O₃ distribution is the depletion of O₃ at ~ 1800 m a.s.l. apparent in the eastern part due to O₃ titration caused by high NO_x emissions from the Bonanza power

Understanding high wintertime ozone pollution events in an oil and natural gas producing region

R. Ahmadov et al.

Title Page

Abstract

Introduction

Conclusions

References

Tables

Figures

◀

▶

◀

▶

Back

Close

Full Screen / Esc

Printer-friendly Version

Interactive Discussion



Understanding high wintertime ozone pollution events in an oil and natural gas producing region

R. Ahmadov et al.

Title Page

Abstract

Introduction

Conclusions

References

Tables

Figures

◀

▶

◀

▶

Back

Close

Full Screen / Esc

Printer-friendly Version

Interactive Discussion

plant. Due to shallow mixing layers at the surface the plume from the power plant's stack does not mix with the air near ground. Photographic evidence during UBWOS-2013 shows thermally buoyant plumes from the Bonanza power plant extending well above the shallow PBL during the stagnant meteorological situations. The WRF-Chem simulation appears to under predict the Bonanza plume rise by ~ 150 m and over predict the vertical spread of the emissions from the power plant. Later we quantify the contribution of the NO_x emissions from this power plant to O_3 at the Horse Pool site within a sensitivity simulation that removes the Bonanza power plant. It is apparent from Fig. 5a and b that the O_3 mixing ratios transported above the UB, advected predominantly by westerly winds, are low, close to background O_3 levels.

Figure 6a and b presents time series of the observed and modeled O_3 vertical distributions over Horse Pool. The observed distribution was obtained by interpolating the eight tethersonde measurements of O_3 for 5 February 2013. The modeled O_3 values were extracted at the time of the vertical profile measurements and then interpolated. The observed temporal variability of O_3 over Horse Pool (Fig. 6a) shows that the strong O_3 buildup starts at $\sim 10:00$ MST and it is confined to a very shallow PBL (~ 100 m thick). The O_3 aloft is found over Horse Pool around 10:00–15:00 MST. The model shows similar characteristics for vertical O_3 profiles during the day. A layer aloft with high O_3 is seen at ~ 350 m above ground in the model. The depletion of O_3 above is caused by titration of O_3 by the Bonanza power plant NO_x emissions at higher altitudes. Figures 5a, b and 6a, b provide insight into the timing, horizontal and vertical distribution of high O_3 observed near the surface and above in the UB. The model predicted vertical distribution of O_3 and its recirculation in the west-east direction within the UB are qualitatively confirmed by the tethersonde measurements taken at Horse Pool. Moreover, the tethersonde comparisons confirm that the Horse Pool surface O_3 measurements are quite representative of the overall O_3 production in the eastern UB, and that the diurnal pattern of O_3 recirculation to Horse Pool is not localized to just that site.

Understanding high wintertime ozone pollution events in an oil and natural gas producing region

R. Ahmadov et al.

Title Page

Abstract

Introduction

Conclusions

References

Tables

Figures

◀

▶

◀

▶

Back

Close

Full Screen / Esc

Printer-friendly Version

Interactive Discussion

In order to verify how well the base model case with the top-down emission scenario simulates O_3 at other locations, Figs. 7a and b show comparisons of O_3 measurements near ground at Ouray and Fantasy Canyon locations (shown on Fig. 1). The observed O_3 concentrations are derived from the tethersonde launches conducted during daytime (09:00–17:00 MST), windowed for the evaluation time period (29 January–8 February 2013). The figures present model O_3 mixing ratios at the times when the tethersonde measurements took place near the ground. The daytime O_3 time series at both sites exhibit a day-to-day variability similar to the Horse Pool measurements. The observed daily maximum O_3 mixing ratios reached ~ 160 ppb at Ouray and ~ 140 ppb at Fantasy Canyon on 5 and 6 February 2013 respectively. Later on maximum daytime O_3 values started decreasing at both sites. The base model case captures the elevated afternoon O_3 concentrations at Ouray and Fantasy canyon quite well. The time series comparisons at all three surface sites show that the WRF-Chem model is able to simulate the spatial and temporal distribution of daytime O_3 in the eastern portion of the UB reasonably well.

4.2 Sensitivity simulations

Here we present different sensitivity simulations to parse out the relative contribution of various factors to O_3 production within the base case simulation. For this purpose we performed multiple model simulations for the same stagnation episode (29 January–8 February 2013) using the same model settings and boundary conditions on the 4 km resolution domain as the base case. These simulations were conducted by applying perturbations to the emissions, photochemical mechanisms and physical processes, while all other settings were kept the same as for the base case simulation. We confine our analysis to O_3 at the Horse Pool site. It should be noted that the sensitivities of O_3 to various perturbations are not additive among the various cases, as the O_3 chemistry is very non-linear.

In order to quantify the impact of the perturbation cases, we use the difference between the base case and the case without the oil/gas emissions (shown in Fig. 3b)

as a normalizing constant. We define impact ratio (IR) for a given simulation case as follows:

$$IR^{\text{case}} = \frac{\left| MB(O_3^{\text{base}}) - MB(O_3^{\text{case}}) \right|}{\left| MB(O_3^{\text{base}}) - MB(O_3^{\text{no oil/gas}}) \right|} \quad (1)$$

Here we use median bias (MB) for O_3 mixing ratios for a given model case as the diagnostic variable. Table 4 presents both MB and IR values for all the model cases discussed hereafter. The IR for the base case (B0) is equal to zero, and the IR for the no oil/gas emissions case is equal to one (B1), per definition.

4.2.1 Sensitivity to the photolysis rates

As discussed in Sect. 3, the WRF-Chem model was modified to include the effect of surface albedo due to surface snow. We tested the model with the same settings as in the base case, but with default bare ground surface albedo conditions used. The test simulation (P1) shows that in this case the IR value is ≈ 1 (Table 4), and this case fails to capture the O_3 production in the UB. Hence, we cannot simulate the high O_3 levels without taking into consideration the enhancement in photolysis rates due to the reflected solar irradiance from the snow cover. This result is similar to the box model cases reported for VOC sensitive regimes for the regions with high oil and NG emissions (Carter and Seinfeld, 2012; Edwards et al., 2013).

We also checked the impact of overhead O_3 column density on the simulated O_3 concentrations at the surface. The case (P2) includes a test simulation, where the column O_3 density was set to 350 DU in the TUV scheme as in the default WRF-Chem code. This 30 % increase reduces modeled O_3 with an IR for this case of 0.22 (Table 4). Thus, model O_3 at Horse Pool is somewhat sensitive to the overhead O_3 column, but the model can still simulate the strong O_3 buildup in the UB.

4.2.2 Sensitivity to the surface deposition processes

As noted in Sect. 3, the presence of a snow layer on the ground also modifies the dry deposition of the gas-phase species. To quantify the contribution of this process to surface O_3 we performed a simulation where the modeled dry deposition velocities for all the gas species are the same as on bare ground, i.e. the default WRF-Chem model. The IR for this case (D1 in Table 4) is significant (0.48). The model in this case still predicts a strong diurnal cycle in O_3 at the surface, but with daytime maximums reduced 20 to 35 ppb.

Another simulation (D2) was done by setting the dry deposition velocity of O_3 to zero in the model. During the UBWOS-2013 field campaign the measured daytime deposition velocities were $\sim 0.002\text{--}0.005\text{ cm s}^{-1}$ over the snowy surface. These values are lower than what the model simulations show for O_3 dry deposition velocities ($\sim 0.02\text{ cm s}^{-1}$) over snowy ground during daytime. Given the possible uncertainty with the O_3 deposition over snow, this test simulation provides us with a low end estimate in terms of O_3 deposition's impact. The simulation shows that if there is no O_3 loss to the ground, the model captures the daytime O_3 concentrations even better than the base case (MB = -0.6 ppb vs. the base case MB of -6.3 ppb) with an IR for this case of 0.19.

4.2.3 Sensitivity to the emission perturbations

Since emissions from the oil/gas sector play a crucial role in driving up O_3 in the UB, we further investigate the influence of various emission scenarios on O_3 at Horse Pool. First, we check the sensitivity of O_3 to possible NO_x (E1) and VOC (E2) emission reductions. This potentially has an important implication for air quality regulations, to find out what emission reduction strategies are more efficient and cost effective to mitigate O_3 exceedances of NAAQS. The E2 simulation in Table 4 reveals that the reduction of VOC emissions by 30 % reduces O_3 nearly one-to-one on a percentage basis (IR = 0.33). Reducing the NO_x emissions from the oil/gas sector by the same amount

Understanding high wintertime ozone pollution events in an oil and natural gas producing region

R. Ahmadov et al.

Title Page

Abstract

Introduction

Conclusions

References

Tables

Figures

◀

▶

◀

▶

Back

Close

Full Screen / Esc

Printer-friendly Version

Interactive Discussion



Understanding high wintertime ozone pollution events in an oil and natural gas producing region

R. Ahmadov et al.

Title Page

Abstract

Introduction

Conclusions

References

Tables

Figures

◀

▶

◀

▶

Back

Close

Full Screen / Esc

Printer-friendly Version

Interactive Discussion

(E1, IR = 0.01) results in essentially no reduction in O₃. The simulation reducing NO_x emissions by a factor of 3 (E4) slightly reduces model O₃ production (IR = 0.14), but is still significantly less effective than the 30 % VOC reduction case E2. It is only when NO_x emissions from the oil/gas sector are completely removed (E5, IR = 0.45) that a significant reduction in O₃ occurs without eliminating any VOCs. We additionally note that when all oil/gas sector NO_x emissions are removed, the model still predicts 2 to 3 ppb daytime NO_x. The remaining NO_x at Horse Pool is 57 % from the towns and highways on the northern edge of the Basin, with the Bonanza power plant accounting for the remainder. Thus, under the high VOC emissions within the UB these levels of NO_x are sufficient to support more than half the O₃ buildup seen in the observations and base case model.

The model case (E6, IR = 0.03) shows that the impact of NO_x emissions from the Bonanza power plant on O₃ concentrations at Horse Pool is very small. This IR is an upper limit since the model appears to under predict the height of the Bonanza source plume as discussed earlier. A model budget of NO_y in the UB deduced from the simulations E5 and E6 shows that 66 % of simulated NO_y is due to oil and gas activity, 10 % is due to the Bonanza power plant, and 24 % is due to vehicle and urban emissions (Vernal and Roosevelt, UT) from the edge of the basin. Again this 10 % contribution from Bonanza can be considered an upper limit to its actual contribution.

Simulations E7 and E8 quantify the contribution of alkane (> C₂) and aromatic VOC species to model O₃ by zeroing out the oil/gas sector emissions for each of these VOC classes. The results show their relative contributions to be nearly the same, and comparable to case E5 where all the oil/gas sector NO_x emissions are removed. Yet, the VOC measurements (Table 3b) and top-down inventory (Table S1) show that aromatic emissions are much smaller than alkane emissions. On a molar basis total aromatic emissions are only ~ 8 % of the emissions of all alkanes having greater than or equal to 5 carbon atoms. The disproportionate impact of oil/gas sector aromatics on wintertime O₃ production has been documented by a box modeling study for another basin, the UGRB in Wyoming (Carter and Seinfeld, 2012).

Understanding high wintertime ozone pollution events in an oil and natural gas producing region

R. Ahmadov et al.

Title Page

Abstract

Introduction

Conclusions

References

Tables

Figures

◀

▶

◀

▶

Back

Close

Full Screen / Esc

Printer-friendly Version

Interactive Discussion



Another uncertainty is the role of primary formaldehyde (CH_2O) emissions. CH_2O is largely produced by photochemistry and has a lifetime less than a couple of hours during midday. Therefore, it is hard to segregate the fraction of CH_2O due to primary emissions using atmospheric measurements. The high correlation of daytime CH_2O with CH_4 (Table S1) could simply be due to photochemical CH_2O formation of correlated primary species. The test simulation (E9, IR = 0.18) shows a moderate impact of the assumed CH_2O emission rate. However, CH_2O is under predicted by 50 % (Table 3b) in the base case simulation that includes the primary emissions.

A modification to the base case simulation was performed to check the impact of the assumed partitioning of oil/gas NO_x emissions between NO , NO_2 and HNO_2 by assuming all NO_x emissions as NO only (E10 case in Table 4). The E10 case results (IR = 0.23) are close to the E9 case (IR = 0.18) suggesting a small 5 % impact related to this assumption about NO_x emission partitioning. This simulation also indicates the insignificant role of primary HNO_2 emissions in simulating high O_3 episode at Horse Pool.

4.2.4 Sensitivity to photochemical processes

It is known that the major hydroxyl radical (OH) production in urban photochemical smog comes from the reaction of atomic oxygen (O^1D) with water vapor (H_2O) molecules. Both H_2O and O_3 (the photolytic source of O^1D) are abundant in polluted urban air in summertime. We checked the importance of this pathway in O_3 production in the UB, by shutting off this reaction in the model. The results indicate that elimination of this pathway (C1 in Table 4) in the model reduces O_3 concentration to some small degree with an IR for this case of 0.25. The model is therefore forming significant O_3 through other radical producing pathways.

Similarly, the model sensitivity to the radical formation channel from CH_2O photolysis was determined by turning off this photolysis reaction (C2 on Table 4). This pathway has twice the impact of the case C1, illustrating the importance of primary and secondary CH_2O as a radical source term within the calculations. Additional radical

sources, primarily dicarbonyls and hydroxy ketones, are the remaining peroxy radical sources contributing to the high modeled O_3 . The radical production from photolysis of various carbonyls for the UBWOS-2013 are studied in detail by Edwards et al. (2014).

Another uncertainty is the loss of NO_x species to particle surfaces. This process depends on aerosol surface area, humidity and other factors. Dinitrogen pentoxide (N_2O_5) formed during the night can participate in heterogeneous aerosol reactions to form nitrate, effectively removing NO_x from the system (Brown et al., 2006). The base case simulation does not include aerosols or any treatment of N_2O_5 conversion to nitrate. In order to estimate an upper limit for the impact of this process, we performed a test simulation in which the chemical reaction between nitrogen trioxide (NO_3) and NO_2 is assumed to yield two HNO_3 molecules directly, rather than through the N_2O_5 intermediate. The results for this case (C3 in Table 4) shows that the model could be somewhat ($IR = 0.19$) sensitive to the treatment of this heterogeneous pathway, but can still simulate high O_3 concentrations under such upper limit assumptions. We note that adding this heterogeneous pathway reduces the positive bias in NO_x seen in the top-down model case in Table 3b. For the time period of the sensitivity runs the median NO_y model to observed ratio is 0.64. By adding the heterogeneous pathway NO_x median model to observed ratios decrease from 1.06 to 0.88, and median of model over observation (MMO) for HNO_3 increase from 0.23 to 0.41, which is more consistent with the magnitude of the 2013 NO_y underprediction.

5 Summary

Our study using the fully coupled meteorology-chemistry WRF-Chem model provides a means to examine the different factors driving high O_3 levels during the wintertime over the UB, Utah from a regional modeling perspective. Two highly contrasting wintertime periods simulate snow-free 2012 and snow-covered 2013. The simulations were performed with two different emission scenarios for O_3 precursors from the oil/gas sector, the bottom-up EPA NEI-2011 (version 1) inventory and a top-down emission esti-

Understanding high wintertime ozone pollution events in an oil and natural gas producing region

R. Ahmadov et al.

Title Page

Abstract

Introduction

Conclusions

References

Tables

Figures

⏪

⏩

◀

▶

Back

Close

Full Screen / Esc

Printer-friendly Version

Interactive Discussion



Understanding high wintertime ozone pollution events in an oil and natural gas producing region

R. Ahmadov et al.

Title Page

Abstract

Introduction

Conclusions

References

Tables

Figures

◀

▶

◀

▶

Back

Close

Full Screen / Esc

Printer-friendly Version

Interactive Discussion

mates based on observed ratios of VOCs and NO_y to CH_4 combined with the observed CH_4 emission rate from Karion et al. (2013). The same meteorological options and domain configuration within the WRF-Chem model were used that adequately simulate conditions during both 2012 and 2013, and most importantly the low wind speeds, low temperatures, and shallow mixing heights associated with cold pool episodes during the winter of 2013. The high resolution 3-D model grid and tight coupling between meteorology and tracer transport in WRF-Chem enables properly simulating the accumulation of the pollutants in shallow mixed layers and their transport aloft over the UB. Air quality models are typically geared towards simulating summertime air quality, and our study shows that if these models properly account for increased photolysis rates and modified surface deposition due to snow cover they can simulate high wintertime O_3 events such as those observed during 2013. Our modeling approach is to use default data sets or observations within a basic model framework to explain high wintertime O_3 with the understanding that simple modifications to assumed emission rates or photochemistry could improve upon the model statistics presented here.

Comparisons of results contrasting the 2012 and 2013 winter simulations show that model O_3 is very insensitive to differences between the bottom-up and top-down scenarios during low O_3 in 2012, but highly sensitive to these differences during 2013, with only the top-down emission data set able to reproduce the observed high O_3 events in 2013. Total oil/gas sector emissions of NO_x are a factor 4 higher, and VOC emissions are 56 % lower, in the bottom-up inventory compared to the top-down inventory in the UB. Statistics for NO_x and VOC species are consistent for both years, showing that the bottom-up inventory yields a high bias in simulated NO_y and nitrogen containing compounds and a low bias for several VOCs. Using the top-down emissions results in much better agreement with the observed precursor levels, though low biases in VOCs and NO_y on the order of 10–30 % are characteristic of the top-down simulations for both years. Under the snow-free conditions of 2012, the meteorological conditions led to effectively coupling air within the UB to air masses further upwind, making O_3 levels less dependent on the local oil/gas sector emissions. In contrast, the cold pool

conditions of 2013 confined locally emitted NO_x and VOCs to very shallow (50–200 m) PBLs, making ground level O_3 quite sensitive to the adopted emission estimates and products, particularly the NO_x/VOC emission ratio.

The CH_4 emission estimate by Karion et al. (2013), which forms the basis of our top-down inventory, is based on a single flight in 2012, which only sampled CH_4 emissions downwind of operations within the eastern part of the UB. Consistent with the NO_x and VOC emissions, the top-down model results show a 10 and 40% low bias for monthly CH_4 statistics in 2012 and 2013, respectively (Table 3a and b). Assuming that meteorology is adequately represented in the model, one would conclude that the Karion et al. (2013) CH_4 flux estimate of $55\,000\text{ kg h}^{-1}$ ($\pm 30\%$), when applied over the entire UB, is a reasonable lower limit. Moreover, NO_x and VOC low biases in the top-down emission case could be eliminated by simply increasing the CH_4 basin-wide emission specification by $\sim 25\%$. By way of contrast, the bottom-up inventory requires significantly larger modifications in order to eliminate NO_y and VOC biases, suggesting a large uncertainty with the methods and numbers used to derive the oil/gas sector emissions found in the NEI-2011 inventory.

A number of perturbation cases to the base model simulation were performed for the 29 January–8 February 2013 high O_3 episode in order to quantify the impact of various model settings, emission reduction scenarios, and photochemical pathways. The impact of meteorological settings applied within the WRF model is not addressed, and left for future work. Since the analysis quantifies the impact on daytime O_3 over an 11 day period, it differs somewhat from the instantaneous reactivity analysis in previous box-model study of oil/gas sector wintertime high O_3 events (Carter and Seinfeld, 2012). The largest O_3 impacts are found to be associated with snow on the ground. Without a high surface albedo, and reduced O_3 deposition velocity induced by the snow cover, the model fails to reproduce the high daytime O_3 observed at a surface site. The 3-D transport and photochemistry formulation afforded by the WRF-Chem model allows the relative importance of snow cover to O_3 deposition to be meaningfully calculated, and it is also found to be a necessary condition for the high O_3 events.

Understanding high wintertime ozone pollution events in an oil and natural gas producing region

R. Ahmadov et al.

Title Page

Abstract

Introduction

Conclusions

References

Tables

Figures

◀

▶

◀

▶

Back

Close

Full Screen / Esc

Printer-friendly Version

Interactive Discussion



Understanding high wintertime ozone pollution events in an oil and natural gas producing region

R. Ahmadov et al.

Title Page

Abstract

Introduction

Conclusions

References

Tables

Figures

◀

▶

◀

▶

Back

Close

Full Screen / Esc

Printer-friendly Version

Interactive Discussion

The emission reduction cases for the high O₃ episode show a large disparity between the impact of NO_x vs. VOCs emission reductions. A 30 % percent reduction in oil/gas NO_x, which reduces median model Horse Pool NO_y concentrations by 23 %, has essentially no impact on the modeled O₃, while the same reduction in VOCs results in an equivalent percentage reduction of O₃ photochemically produced. The impact of NO_x reductions is found to be very nonlinear, with reductions showing significant O₃ impact only after the first 2/3 of the specified oil/gas sector NO_x emissions are removed. The importance of alkane vs. aromatic VOC emissions is tested within simulations that eliminate each class of VOCs separately. O₃ formation is reduced significantly and to roughly the same degree in both cases, despite the fact that aromatic VOC emissions are less than 10 % of the C5 and greater alkane emissions from the oil/gas sector on a molar basis. Our results suggest that efforts to reduce wintertime O₃ from the oil/gas sector through VOC reductions would benefit the most by targeting the aromatic compounds. The sensitivity simulation without primary CH₂O emissions indicates that it is important to quantify the sources of primary CH₂O from the oil and NG production. An additional simulation demonstrates the importance of CH₂O photolysis to the radical chemistry. Another important conclusion from our study is that high O₃ concentrations can be simulated without direct emissions of HNO₂, which was previously considered a potential radical source in snowy conditions.

The results from this study point to several future refinements that may be necessary in order to better simulate the meteorological and photochemical processes pertinent to the wintertime conditions. Although using emissions based on observations offers significant improvement over the bottom-up emissions inventory, there are potentially important details missing in the top-down emission estimates. Speciation profiles for oil vs. NG wells, and other stationary sources, are known to be different (Warneke et al., 2014). Also, the same emissions are used for both 2012 and 2013, neglecting any temporal variability in overall oil and NG production. Thus, a synergy between bottom-up and top-down approaches will be needed in order to develop more accurate emission inventories for the oil/gas sector in the US. Moreover, as Carter and Seinfeld (2012)

pointed out at present there is insufficient information available to adapt gas-phase chemistry mechanisms to cold conditions, particularly for aromatic VOCs. We would further recommend additional laboratory and field studies related to heterogeneous and deposition processes occurring at low air temperatures over snowy surfaces.

The 3-D model framework and top-down emission estimates presented here provide a unique set of tools to help better understand and quantify the major factors determining high wintertime O₃ levels within the Uinta Basin, UT and in other oil and natural gas production regions with potentially similar conditions.

**The Supplement related to this article is available online at
doi:10.5194/acpd-14-20295-2014-supplement.**

Acknowledgements. Part of this work (R. Ahmadov and S. McKeen) is supported by the US Weather Research Program within NOAA/OAR Office of Weather and Air Quality. The authors thank David Parrish (NOAA and CU Boulder), Gail Tonnesen (EPA) and Seth Lyman (Utah State University) for useful discussions. We wish to thank Georg Grell and Steven Peckham (NOAA and CU Boulder) for the user support of the WRF-Chem model. Measurements were funded in part by the Western Energy Alliance and NOAA's Climate and Health of the Atmosphere programs. The contents of this paper reflect only the opinions of the authors, and not necessarily those of National Oceanic and Atmospheric Administration, or any other individuals or organizations mentioned herein.

References

Ahmadov, R., McKeen, S. A., Robinson, A. L., Bahreini, R., Middlebrook, A. M., de Gouw, J. A., Meagher, J., Hsie, E. Y., Edgerton, E., Shaw, S., and Trainer, M.: A volatility basis set model for summertime secondary organic aerosols over the eastern United States in 2006, *J. Geophys. Res.-Atmos.*, 117, D06301, doi:10.1029/2011jd016831, 2012.

Understanding high wintertime ozone pollution events in an oil and natural gas producing region

R. Ahmadov et al.

Title Page

Abstract

Introduction

Conclusions

References

Tables

Figures



Back

Close

Full Screen / Esc

Printer-friendly Version

Interactive Discussion



Understanding high wintertime ozone pollution events in an oil and natural gas producing region

R. Ahmadov et al.

Title Page

Abstract

Introduction

Conclusions

References

Tables

Figures

◀

▶

◀

▶

Back

Close

Full Screen / Esc

Printer-friendly Version

Interactive Discussion

- Alvarez, R. A., Pacala, S. W., Winebrake, J. J., Chameides, W. L., and Hamburg, S. P.: Greater focus needed on methane leakage from natural gas infrastructure, *P. Natl. Acad. Sci. USA*, 109, 6435–6440, doi:10.1073/pnas.1202407109, 2012.
- 5 Anenberg, S. C., Horowitz, L. W., Tong, D. Q., and West, J. J.: An estimate of the global burden of anthropogenic ozone and fine particulate matter on premature human mortality using atmospheric modeling, *Environ. Health Persp.*, 118, 1189–1195, doi:10.1289/ehp.0901220, 2010.
- Baker, K. R., Simon, H., and Kelly, J. T.: Challenges to modeling “Cold Pool” meteorology associated with high pollution episodes, *Environ. Sci. Technol.*, 45, 7118–7119, doi:10.1021/es202705v, 2011.
- 10 Banta, R. and Cotton, W. R.: An analysis of the structure of local wind systems in a broad mountain basin, *J. Appl. Meteorol.*, 20, 1255–1266, doi:10.1175/1520-0450(1981)020<1255:aaotso>2.0.co;2, 1981.
- Banta, R. M., Senff, C. J., Alvarez, R. J., Langford, A. O., Parrish, D. D., Trainer, M. K., Darby, L. S., Hardesty, R. M., Lambeth, B., Neuman, J. A., Angevine, W. M., Nielsen-Gammon, J., Sandberg, S. P., and White, A. B.: Dependence of daily peak O₃ concentrations near Houston, Texas on environmental factors: wind speed, temperature, and boundary-layer depth, *Atmos. Environ.*, 45, 162–173, doi:10.1016/j.atmosenv.2010.09.030, 2011.
- 15 Brandt, A. R., Heath, G. A., Kort, E. A., O’Sullivan, F., Pétron, G., Jordaan, S. M., Tans, P., Wilcox, J., Gopstein, A. M., Arent, D., Wofsy, S., Brown, N. J., Bradley, R., Stucky, G. D., Eardley, D., and Harriss, R.: Methane leaks from North American natural gas systems, *Science*, 343, 733–735, doi:10.1126/science.1247045, 2014.
- Brioude, J., Angevine, W. M., Ahmadov, R., Kim, S.-W., Evan, S., McKeen, S. A., Hsie, E.-Y., Frost, G. J., Neuman, J. A., Pollack, I. B., Peischl, J., Ryerson, T. B., Holloway, J., Brown, S. S., Nowak, J. B., Roberts, J. M., Wofsy, S. C., Santoni, G. W., Oda, T., and Trainer, M.: Top-down estimate of surface flux in the Los Angeles Basin using a mesoscale inverse modeling technique: assessing anthropogenic emissions of CO, NO_x and CO₂ and their impacts, *Atmos. Chem. Phys.*, 13, 3661–3677, doi:10.5194/acp-13-3661-2013, 2013.
- 25 Brown, S. S., Neuman, J. A., Ryerson, T. B., Trainer, M., Dube, W. P., Holloway, J. S., Warneke, C., de Gouw, J. A., Donnelly, S. G., Atlas, E., Matthew, B., Middlebrook, A. M., Peltier, R., Weber, R. J., Stohl, A., Meagher, J. F., Fehsenfeld, F. C., and Ravishankara, A. R.: Nocturnal odd-oxygen budget and its implications for ozone loss in the lower troposphere, *Geophys. Res. Lett.*, 33, L08801, doi:10.1029/2006gl025900, 2006.
- 30

Understanding high wintertime ozone pollution events in an oil and natural gas producing region

R. Ahmadov et al.

Title Page

Abstract

Introduction

Conclusions

References

Tables

Figures

◀

▶

◀

▶

Back

Close

Full Screen / Esc

Printer-friendly Version

Interactive Discussion



Carlton, A. G., Little, E., Moeller, M., Odoyo, S., and Shepson, P. B.: The Data Gap: can a Lack of monitors obscure loss of clean air act benefits in fracking areas?, *Environ. Sci. Technol.*, 48, 893–894, doi:10.1021/es405672t, 2014.

Carter, W. P. L. and Seinfeld, J. H.: Winter ozone formation and VOC incremental reactivities in the Upper Green River Basin of Wyoming, *Atmos. Environ.*, 50, 255–266, doi:10.1016/j.atmosenv.2011.12.025, 2012.

Clements, C. B., Whiteman, C. D., and Horel, J. D.: Cold-air-pool structure and evolution in a mountain basin: Peter Sinks, Utah, *J. Appl. Meteorol.*, 42, 752–768, doi:10.1175/1520-0450(2003)042<0752:csaeia>2.0.co;2, 2003.

Cooper, O. R., Gao, R. S., Tarasick, D., Leblanc, T., and Sweeney, C.: Long-term ozone trends at rural ozone monitoring sites across the United States, 1990–2010, *J. Geophys. Res.-Atmos.*, 117, D22307, doi:10.1029/2012jd018261, 2012.

de Gouw, J. A., Parrish, D. D., Frost, G. J., and Trainer, M.: Reduced emissions of CO₂, NO_x, and SO₂ from US power plants owing to switch from coal to natural gas with combined cycle technology, *Earth's Future*, 2, 75–82, doi:10.1002/2013ef000196, 2014.

Dibb, J. E., Talbot, R. W., Munger, J. W., Jacob, D. J., and Fan, S. M.: Air-snow exchange of HNO₃ and NO_y at Summit, Greenland, *J. Geophys. Res.-Atmos.*, 103, 3475–3486, doi:10.1029/97jd03132, 1998.

Edwards, P. M., Young, C. J., Aikin, K., deGouw, J., Dubé, W. P., Geiger, F., Gilman, J., Helmig, D., Holloway, J. S., Kercher, J., Lerner, B., Martin, R., McLaren, R., Parrish, D. D., Peischl, J., Roberts, J. M., Ryerson, T. B., Thornton, J., Warneke, C., Williams, E. J., and Brown, S. S.: Ozone photochemistry in an oil and natural gas extraction region during winter: simulations of a snow-free season in the Uintah Basin, Utah, *Atmos. Chem. Phys.*, 13, 8955–8971, doi:10.5194/acp-13-8955-2013, 2013.

Edwards, P. M., Brown, S., Roberts, J., Ahmadov, R., Banta, R., de Gouw, J., Dubé, W., Field, R., Flynn, J., Gilman, J., Graus, M., Helmig, D., Koss, A., Langford, A., Lefer, B., Lerner, B., Li, R., Li, S., McKeen, S., Murphy, S., Parrish, D., Senff, C., Soltis, J., Stutz, J., Sweeney, C., Thompson, C., Trainer, M., Tsai, C., Veres, P., Washenfelder, R., Warneke, C., Wild, R., Young, C., Yuan, B., Zamora, R.: Unconventional photochemistry underlying winter ozone in an oil and gas producing region, *Nature*, submitted, 2014.

Erismann, J. W., Vanpul, A., and Wyers, P.: Parametrization of surface-resistance for the quantification of atmospheric deposition of acidifying pollutants and ozone, *Atmos. Environ.*, 28, 2595–2607, 1994.

Understanding high wintertime ozone pollution events in an oil and natural gas producing region

R. Ahmadov et al.

Title Page

Abstract

Introduction

Conclusions

References

Tables

Figures

◀

▶

◀

▶

Back

Close

Full Screen / Esc

Printer-friendly Version

Interactive Discussion



- Gilman, J. B., Lerner, B. M., Kuster, W. C., and de Gouw, J. A.: Source signature of Volatile Organic Compounds from oil and natural gas operations in northeastern Colorado, *Environ. Sci. Technol.*, 47, 1297–1305, doi:10.1021/es304119a, 2013.
- 5 Grell, G. A., Peckham, S. E., Schmitz, R., McKeen, S. A., Frost, G., Skamarock, W. C., and Eder, B.: Fully coupled “online” chemistry within the WRF model, *Atmos. Environ.*, 39, 6957–6975, doi:10.1016/j.atmosenv.2005.04.027, 2005.
- Helmig, D., Thompson, C. R., Evans, J., Boylan, P., Hueber, J., and Park, J. H.: Highly elevated atmospheric levels of Volatile Organic Compounds in the Uintah Basin, Utah, *Environ. Sci. Technol.*, 48, 4707–4715, doi:10.1021/es405046r, 2014.
- 10 Jackson, R. B., Down, A., Phillips, N. G., Ackley, R. C., Cook, C. W., Plata, D. L., and Zhao, K. G.: Natural gas pipeline leaks across Washington, DC, *Environ. Sci. Technol.*, 48, 2051–2058, doi:10.1021/es404474x, 2014.
- Jerrett, M., Burnett, R. T., Pope, C. A., Ito, K., Thurston, G., Krewski, D., Shi, Y. L., Calle, E., and Thun, M.: Long-term ozone exposure and mortality, *New Engl. J. Med.*, 360, 1085–1095, doi:10.1056/NEJMoa0803894, 2009.
- 15 Johansson, C. and Granat, L.: An experimental-study of the dry deposition of gaseous nitric acid to snow, *Atmos. Environ.*, 20, 1165–1170, doi:10.1016/0004-6981(86)90150-2, 1986.
- Karion, A., Sweeney, C., Pétron, G., Frost, G., Hardesty, R. M., Kofler, J., Miller, B. R., Newberger, T., Wolter, S., Banta, R., Brewer, A., Dlugokencky, E., Lang, P., Montzka, S. A., Schnell, R., Tans, P., Trainer, M., Zamora, R., and Conley, S.: Methane emissions estimate from airborne measurements over a western United States natural gas field, *Geophys. Res. Lett.*, 40, 4393–4397, doi:10.1002/grl.50811, 2013.
- 20 Katzenstein, A. S., Doezema, L. A., Simpson, I. J., Balke, D. R., and Rowland, F. S.: Extensive regional atmospheric hydrocarbon pollution in the southwestern United States, *P. Natl. Acad. Sci. USA*, 100, 11975–11979, doi:10.1073/pnas.1635258100, 2003.
- Kemball-Cook, S., Bar-Ilan, A., Grant, J., Parker, L., Jung, J. G., Santamaria, W., Mathews, J., and Yarwood, G.: Ozone impacts of natural gas development in the Haynesville Shale, *Environ. Sci. Technol.*, 44, 9357–9363, doi:10.1021/es1021137, 2010.
- 25 Kim, S. W., Heckel, A., Frost, G. J., Richter, A., Gleason, J., Burrows, J. P., McKeen, S., Hsie, E. Y., Granier, C., and Trainer, M.: NO₂ columns in the western United States observed from space and simulated by a regional chemistry model and their implications for NO_x emissions, *J. Geophys. Res.-Atmos.*, 114, D11301, doi:10.1029/2008jd011343, 2009.
- 30

Understanding high wintertime ozone pollution events in an oil and natural gas producing region

R. Ahmadov et al.

Title Page

Abstract

Introduction

Conclusions

References

Tables

Figures

◀

▶

◀

▶

Back

Close

Full Screen / Esc

Printer-friendly Version

Interactive Discussion



- Kim, S.-W., McKeen, S. A., Frost, G. J., Lee, S.-H., Trainer, M., Richter, A., Angevine, W. M., Atlas, E., Bianco, L., Boersma, K. F., Brioude, J., Burrows, J. P., de Gouw, J., Fried, A., Gleason, J., Hilboll, A., Mellqvist, J., Peischl, J., Richter, D., Rivera, C., Ryerson, T., te Lin-
tel Hekkert, S., Walega, J., Warneke, C., Weibring, P., and Williams, E.: Evaluations of NO_x
and highly reactive VOC emission inventories in Texas and their implications for ozone plume
simulations during the Texas Air Quality Study 2006, *Atmos. Chem. Phys.*, 11, 11361–11386,
doi:10.5194/acp-11-11361-2011, 2011.
- Lareau, N. P., Crosman, E., Whiteman, C. D., Horel, J. D., Hoch, S. W., Brown, W. O. J.,
and Horst, T. W.: The persistent cold-air pool study, *B. Am. Meteorol. Soc.*, 94, 51–63,
doi:10.1175/bams-d-11-00255.1, 2013.
- Lelieveld, J. and Dentener, F. J.: What controls tropospheric ozone?, *J. Geophys. Res.-Atmos.*,
105, 3531–3551, doi:10.1029/1999jd901011, 2000.
- Madronich, S.: Photodissociation in the atmosphere, 1. Actinic flux and the ef-
fects of ground reflections and clouds, *J. Geophys. Res.-Atmos.*, 92, 9740–9752,
doi:10.1029/JD092iD08p09740, 1987.
- Miller, S. M., Wofsy, S. C., Michalak, A. M., Kort, E. A., Andrews, A. E., Biraud, S. C., Dlu-
gokencky, E. J., Eluszkiewicz, J., Fischer, M. L., Janssens-Maenhout, G., Miller, B. R.,
Miller, J. B., Montzka, S. A., Nehr Korn, T., and Sweeney, C.: Anthropogenic emis-
sions of methane in the United States, *P. Natl. Acad. Sci. USA*, 110, 20018–20022,
doi:10.1073/pnas.1314392110, 2013.
- Oltmans, S. J., Schnell, R. C., Johnson, B. J., Pétron, G., Mefford, T., Neely III, R.: Anatomy of
wintertime ozone production associated with oil and gas extraction activity in Wyoming and
Utah, *Elem. Sci. Anth.*, 2, 000024, doi:10.12952/journal.elementa.000024, 2014.
- Pétron, G., Frost, G., Miller, B. R., Hirsch, A. I., Montzka, S. A., Karion, A., Trainer, M.,
Sweeney, C., Andrews, A. E., Miller, L., Kofler, J., Bar-Ilan, A., Dlugokencky, E. J., Patrick, L.,
Moore, C. T., Ryerson, T. B., Siso, C., Kolodzey, W., Lang, P. M., Conway, T., Novelli, P.,
Masarie, K., Hall, B., Guenther, D., Kitzis, D., Miller, J., Welsh, D., Wolfe, D., Neff, W.,
and Tans, P.: Hydrocarbon emissions characterization in the Colorado Front Range: a pi-
lot study, *J. Geophys. Res.-Atmos.*, 117, D04304, doi:10.1029/2011jd016360, 2012.
- Pétron, G., Karion, A., Sweeney, C., Miller, B., Montzka, S., Frost, G., Trainer, M., Tans, P.,
Andrews, A., Kofler, J., Helmig, D., Guenther, D., Dlugokencky, E., Lang, P., Newberger, T.,
Wolter, S., Hall, B., Novelli, P., Brewer, A., Conley, S., Hardesty, M., Banta, R., White, A.,
Noone, D., Wolfe, D., and Schnell, R.: A new look at methane and nonmethane hydrocarbon

Understanding high wintertime ozone pollution events in an oil and natural gas producing region

R. Ahmadov et al.

Title Page

Abstract

Introduction

Conclusions

References

Tables

Figures

◀

▶

◀

▶

Back

Close

Full Screen / Esc

Printer-friendly Version

Interactive Discussion



emissions from oil and natural gas operations in the Colorado Denver-Julesburg Basin, *J. Geophys. Res.-Atmos.*, 119, 6836–6852, doi:10.1002/2013JD021272, 2014.

Rappenglück, B., Ackermann, L., Alvarez, S., Golovko, J., Buhr, M., Field, R. A., Soltis, J., Montague, D. C., Hauze, B., Adamson, S., Risch, D., Wilkerson, G., Bush, D., Stoeckenius, T., and Keslar, C.: Strong wintertime ozone events in the Upper Green River basin, Wyoming, *Atmos. Chem. Phys.*, 14, 4909–4934, doi:10.5194/acp-14-4909-2014, 2014.

Reeves, H. D. and Stensrud, D. J.: Synoptic-scale flow and valley cold pool evolution in the western United States, *Weather Forecast.*, 24, 1625–1643, doi:10.1175/2009waf2222234.1, 2009.

Rodriguez, M. A., Barna, M. G., and Moore, T.: Regional impacts of oil and gas development on ozone formation in the western United States, *J. Air Waste Manage.*, 59, 1111–1118, doi:10.3155/1047-3289.59.9.1111, 2009.

Roy, A. A., Adams, P. J., and Robinson, A. L.: Air pollutant emissions from the development, production, and processing of Marcellus Shale natural gas, *J. Air Waste Manage.*, 64, 19–37, doi:10.1080/10962247.2013.826151, 2014.

Ryerson, T. B., Trainer, M., Angevine, W. M., Brock, C. A., Dissly, R. W., Fehsenfeld, F. C., Frost, G. J., Goldan, P. D., Holloway, J. S., Hübler, G., Jakoubek, R. O., Kuster, W. C., Neuman, J. A., Nicks, D. K., Jr., Parrish, D. D., Roberts, J. M., Sueper, D. T., Atlas, E. L., Donnelly, S. G., Flocke, F., Fried, A., Potter, W. T., Schauffler, S., Stroud, V., Weinheimer, A. J., Wert, B. P., Wiedinmyer, C., Alvarez, R. J., Banta, R. M., Darby, L. S., and Senff, C. J.: Effect of petrochemical industrial emissions of reactive alkenes and NO_x on tropospheric ozone formation in Houston, Texas, *J. Geophys. Res.*, 108, 4249, doi:10.1029/2002JD003070, 2003.

Schnell, R. C., Oltmans, S. J., Neely, R. R., Endres, M. S., Molenaar, J. V., and White, A. B.: Rapid photochemical production of ozone at high concentrations in a rural site during winter, *Nat. Geosci.*, 2, 120–122, doi:10.1038/ngeo415, 2009.

Simon, H., Beck, L., Bhave, P. V., Divita, F., Hsu, Y., Luecken, D., Mobley, J. D., Pouliot, G. A., Reff, A., Sarwar, G., and Strum, M.: The development and uses of EPA's SPECIATE database, *Atmos. Pollut. Res.*, 1, 196–206, doi:10.5094/apr.2010.026, 2010.

Stockwell, W. R., Kirchner, F., Kuhn, M., and Seefeld, S.: A new mechanism for regional atmospheric chemistry modeling, *J. Geophys. Res.-Atmos.*, 102, 25847–25879, 1997.

Trainer, M., Parrish, D. D., Goldan, P. D., Roberts, J., and Fehsenfeld, F. C.: Review of observation-based analysis of the regional factors influencing ozone concentrations, *Atmos. Environ.*, 34, 2045–2061, 2000.

Warneke, C., Geiger, F., Edwards, P. M., Dube, W., Pétron, G., Kofler, J., Zahn, A., Brown, S. S., Graus, M., Gilman, J., Lerner, B., Peischl, J., Ryerson, T. B., de Gouw, J. A., and Roberts, J. M.: Volatile organic compound emissions from the oil and natural gas industry in the Uinta Basin, Utah: point sources compared to ambient air composition, Atmos. Chem. Phys. Discuss., 14, 11895–11927, doi:10.5194/acpd-14-11895-2014, 2014.

5

Understanding high wintertime ozone pollution events in an oil and natural gas producing region

R. Ahmadov et al.

Title Page

Abstract

Introduction

Conclusions

References

Tables

Figures



Back

Close

Full Screen / Esc

Printer-friendly Version

Interactive Discussion



Understanding high wintertime ozone pollution events in an oil and natural gas producing region

R. Ahmadov et al.

Title Page

Abstract

Introduction

Conclusions

References

Tables

Figures

◀

▶

◀

▶

Back

Close

Full Screen / Esc

Printer-friendly Version

Interactive Discussion

Table 1. List of acronyms used in the text.

Acronym	Description
3-D	Three dimensional
ASL	Above sea level
CB	Carbon Bond
DU	Dobson unit
EPA	Environmental Protection Agency
IR	Impact ratio
MB	Median bias
MMO	Median of model over observation
MO	Median of observations
MST	Mountain Standard Time
NAAQS	National Ambient Air Quality Standards
NOAA	National Oceanic and Atmospheric Administration
NEI	National Emissions Inventory
NG	Natural gas
PBL	Planetary boundary layer
ppb	parts per billion
RACM	Regional Atmospheric Chemistry Mechanism
SI	Supplemental Information
UB	Uinta Basin
UBWOS	Uinta Basin Winter Ozone Study
UGRB	Upper Green River Basin
VCPs	Valley cold pools
VOCs	Volatile organic compounds
WRF-Chem	Weather Research and Forecasting with Chemistry

Understanding high wintertime ozone pollution events in an oil and natural gas producing region

R. Ahmadov et al.

Table 2. Anthropogenic emission estimates for Duchesne and Uintah Counties based on the EPA NEI-2011, NEI-2005 and the top-down estimates for oil and gas operations alone. “All Other Activity” excludes the Bonanza Power Plant emissions. NO_x emissions are in tons/year of NO₂ equivalent.

Emissions scenarios	Source and methods	Emission sectors	NO _x (short t year ⁻¹)	Total VOC (short t year ⁻¹)	CH ₄ (short t year ⁻¹)
Bottom-up	NEI-2011	Oil and Gas	18 131	111 536	110 539
		All other Activity	4514	3047	1597
		Bonanza Power Plant	6590	46	–
Top-down	Regression analysis	Oil and Gas	4583	203 389	531 457
	NEI-2005	All other Activity	2585	3525	1231
		Bonanza Power Plant	6712	63	–

Title Page

Abstract

Introduction

Conclusions

References

Tables

Figures

◀

▶

◀

▶

Back

Close

Full Screen / Esc

Printer-friendly Version

Interactive Discussion

Understanding high wintertime ozone pollution events in an oil and natural gas producing region

R. Ahmadov et al.

Table 3a. Statistics for observed and simulated chemical species mixing ratios at Horse Pool, daytime 09:00–17:00 MST hourly average observations for the two UBWOS campaigns, 31 January–28 February 2012; N – number of used hourly observations, MO – median of observations, r – Pearson correlation coefficient, MB – median model-observation bias, MMO – median of model over observation.

Gas species	N	MO (ppb)	Bottom-up (NEI-2011)			Top-Down		
			r	MB (ppb)	MMO	r	MB (ppb)	MMO
Ozone (O_3)	261	35.94	0.79	0.24	1.01	0.77	3.64	1.11
Odd oxygen (= $O_3 + NO_2$)	162	36.79	0.69	2.83	1.08	0.76	4.08	1.11
Nitrogen oxides (NO_x)	162	4.79	0.60	2.92	1.85	0.59	-0.83	0.75
Reactive odd nitrogen (NO_y)	224	4.81	0.67	1.50	1.55	0.64	-0.96	0.70
NO_z (= $NO_y - NO_x$)	160	1.73	0.00	-0.51	0.67	0.11	-0.44	0.69
Methane (CH_4)	261	2509.0	0.65	-704.9	0.73	0.65	-211.3	0.90
Ethane (C_2H_6)	228	49.29	0.65	-30.12	0.38	0.65	-7.74	0.73
Toluene (C_7H_8)	254	0.63	0.65	-0.34	0.39	0.64	-0.05	0.87
Xylene (C_8H_{10})	254	0.32	0.65	-0.24	0.24	0.64	-0.07	0.71
Propene (C_3H_6)	228	0.04	0.69	-0.01	0.64	0.67	-0.02	0.38
Ethene (C_2H_4)	228	0.38	0.48	-0.35	0.07	0.67	-0.15	0.50
Formaldehyde (CH_2O)	254	1.32	0.23	-0.72	0.46	0.52	-0.41	0.67
Acetaldehyde (CH_3CHO)	254	0.42	0.54	-0.12	0.67	0.58	0.46	2.01
Nitric acid (HNO_3)	252	0.50	0.38	0.03	1.12	0.41	-0.07	0.82
Peroxyacetyl nitrate (PAN)	236	0.32	0.53	-0.17	0.43	0.62	-0.12	0.61

Understanding high wintertime ozone pollution events in an oil and natural gas producing region

R. Ahmadov et al.

Table 3b. Statistics for observed and simulated chemical species mixing ratios at Horse Pool, daytime 09:00–17:00 MST hourly average observations for the two UBWOS campaigns, 29 January–22 February 2013; N – number of used hourly observations, MO – median of observations, r – Pearson correlation coefficient, MB – median model-observation bias, MMO – median of model over observation.

Gas species	N	MO (ppb)	Bottom-up			Top-Down		
			r	MB (ppb)	MMO	r	MB (ppb)	MMO
Ozone (O_3)	191	81.88	0.33	−39.80	0.51	0.85	−5.25	0.93
Odd oxygen (= $O_3 + NO_2$)	191	85.82	0.83	−29.19	0.67	0.85	−4.65	0.95
Nitrogen oxides (NO_x)	193	4.93	−0.02	22.25	5.39	0.25	0.86	1.19
Reactive odd nitrogen (NO_y)	154	17.16	0.35	13.92	1.86	0.46	−4.50	0.75
NO_z (= $NO_y - NO_x$)	154	12.82	0.40	−9.29	0.26	0.50	−5.71	0.54
Methane (CH_4)	210	7340.0	0.29	−5100.0	0.31	0.37	−2913.0	0.61
Ethane (C_2H_6)	178	320.74	0.40	−223.95	0.24	0.48	−148.22	0.53
Toluene (C_7H_8)	204	4.01	0.32	−2.95	0.24	0.44	−1.78	0.55
Xylene (C_8H_{10})	204	1.66	0.30	−1.35	0.17	0.44	−0.90	0.43
Propene (C_3H_6)	192	0.20	0.23	−0.09	0.54	0.16	−0.14	0.22
Ethene (C_2H_4)	192	2.26	0.24	−2.21	0.02	0.43	−1.44	0.35
Formaldehyde (CH_2O)	204	4.85	0.12	−3.82	0.18	0.10	−2.34	0.53
Acetaldehyde (CH_3CHO)	204	4.41	0.70	−2.79	0.35	0.73	1.03	1.27
Nitric acid (HNO_3)	179	4.46	0.18	−2.77	0.35	0.22	−3.05	0.26
Peroxyacetyl nitrate (PAN)	200	2.00	0.78	−1.66	0.20	0.78	−0.11	0.90

Understanding high wintertime ozone pollution events in an oil and natural gas producing region

R. Ahmadov et al.

Title Page

Abstract

Introduction

Conclusions

References

Tables

Figures

◀

▶

◀

▶

Back

Close

Full Screen / Esc

Printer-friendly Version

Interactive Discussion



Table 4. Median bias (MB) and impact ratio (IR) for O₃ at Horse Pool for various perturbations to the base model. Model results are compared against hourly average observations between 09:00–17:00 MST, 29 January–8 February 2013.

Modeling case ID	Model perturbation case	MB (ppb)	IR
B0	Base simulation (top-down emissions)	−6.32	–
B1	Base simulation, all oil/gas emissions set to zero	−35.81	1.00
	Photolysis		
P1	Snow albedo replaced by bare-ground albedo	−37.06	1.04
P2	Overhead column O ₃ increased by 30 %	−12.94	0.22
	Deposition		
D1	No snow effect on dry deposition of gas species	−20.49	0.48
D2	O ₃ deposition velocity set to zero	−0.62	0.19
	Emissions		
E1	Oil/gas NO _x emissions decreased by 30 %	−6.57	0.01
E2	Oil/gas VOC emissions decreased by 30 %	−16.06	0.33
E3	Oil/gas NO _x and VOC emissions decreased by 30 %	−14.23	0.27
E4	Oil/gas NO _x emissions decreased by 66.67 %	−10.42	0.14
E5	Oil/gas NO _x emissions set to zero	−19.56	0.45
E6	Bonanza power plant NO _x emissions removed	−7.22	0.03
E7	Oil/gas alkane (> C2) VOC emissions set to zero	−19.41	0.44
E8	Oil/gas aromatic VOC emissions set to zero	−17.15	0.37
E9	Oil/gas CH ₂ O emissions set to zero	−11.66	0.18
E10	Oil/gas CH ₂ O emissions, HNO ₂ and NO ₂ in NO _x emissions set to zero	−13.09	0.23
	Chemistry		
C1	O ¹ D + H ₂ O → 2OH reaction rate set to zero	−13.66	0.25
C2	CH ₂ O + hν → CO + 2HO ₂ photolysis channel set to zero	−21.42	0.52
C3	NO ₃ + NO ₂ → 2HNO ₃ (heterogeneous NO _x loss upper limit)	−11.96	0.19

Understanding high wintertime ozone pollution events in an oil and natural gas producing region

R. Ahmadov et al.

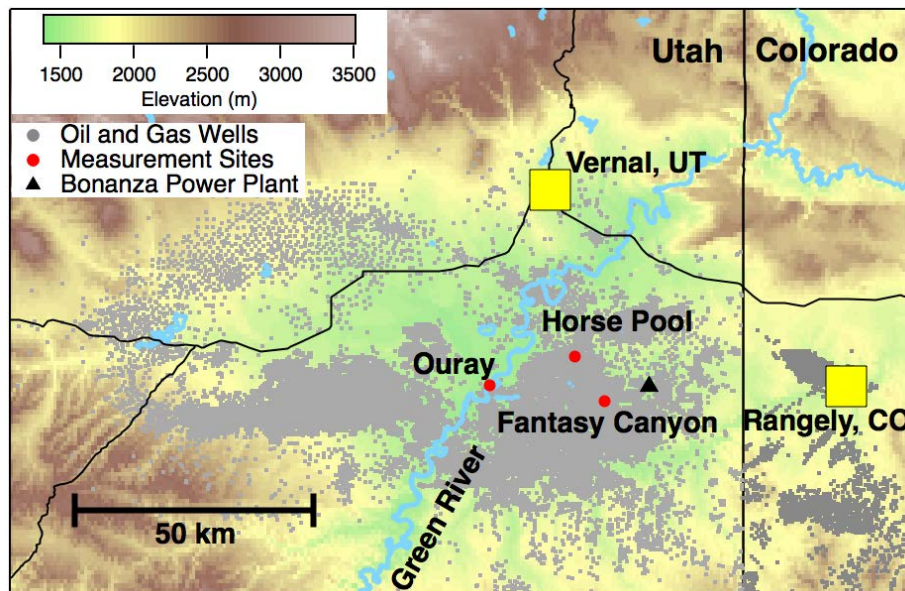


Figure 1. Topography of the Uinta Basin, UT. The locations of oil and NG wells, measurement sites – Ouray (40.1348° N, 109.6446° W), Horse Pool (40.1431° N, 109.4674° W) and Fantasy Canyon (40.0582° N, 109.3941° W) during the UBWOS-2013 field campaign, Bonanza power plant (40.0864° N, 109.2844° W) and towns (Vernal, UT and Rangely, CO) are also shown.

Title Page

Abstract

Introduction

Conclusions

References

Tables

Figures

◀

▶

◀

▶

Back

Close

Full Screen / Esc

Printer-friendly Version

Interactive Discussion

Understanding high wintertime ozone pollution events in an oil and natural gas producing region

R. Ahmadov et al.

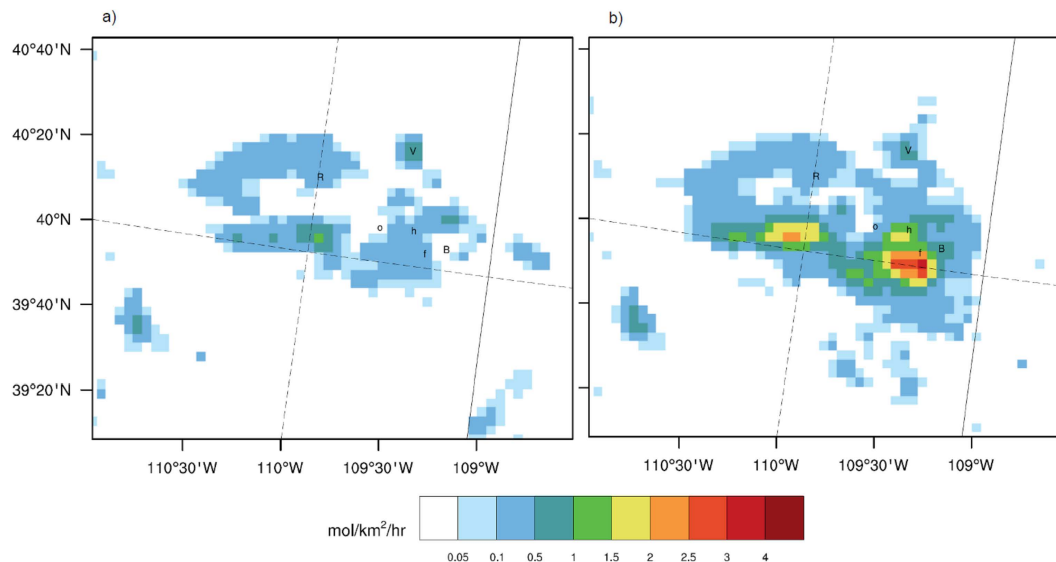


Figure 2. 24 h averaged anthropogenic emissions of toluene in the Uinta Basin and surroundings; **(a)** bottom-up (NEI-2011) inventory; **(b)** top-down emission dataset. The letters point to the surface measurement sites: o – Ouray, h – Horse Pool and f – Fantasy Canyon; power plant: B – Bonanza, towns R – Roosevelt and V – Vernal. The solid line is a border between Colorado and Utah states.

Understanding high wintertime ozone pollution events in an oil and natural gas producing region

R. Ahmadov et al.

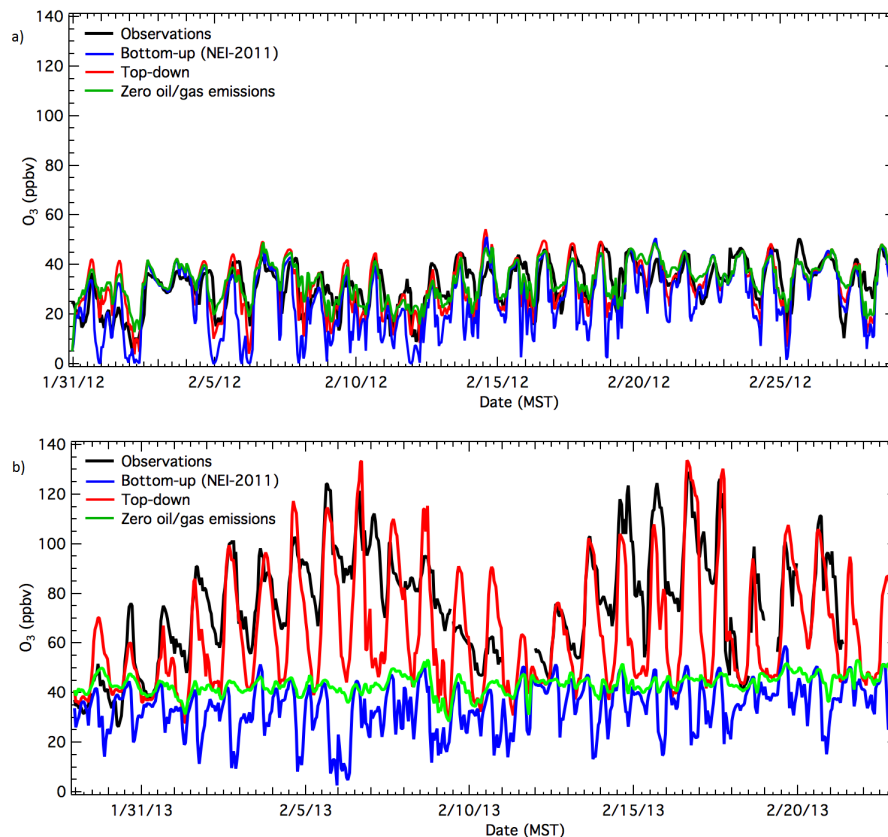


Figure 3. Time series of the measured and modeled hourly O_3 mixing ratios at Horse Pool in (a) 2012, (b) 2013.

Understanding high wintertime ozone pollution events in an oil and natural gas producing region

R. Ahmadov et al.

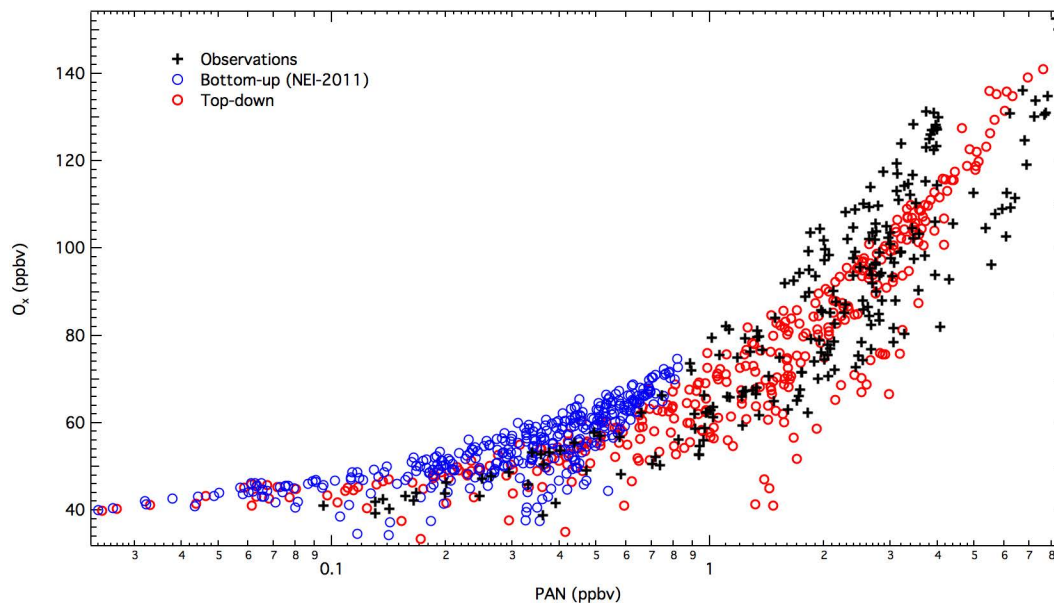


Figure 4. Scatter plot of measured and modeled hourly O_x vs. PAN mixing ratios during daytime (09:00–17:00 MST), 29 January–22 February 2013 at Horse Pool.

Title Page

Abstract

Introduction

Conclusions

References

Tables

Figures

◀

▶

◀

▶

Back

Close

Full Screen / Esc

Printer-friendly Version

Interactive Discussion

Understanding high wintertime ozone pollution events in an oil and natural gas producing region

R. Ahmadov et al.

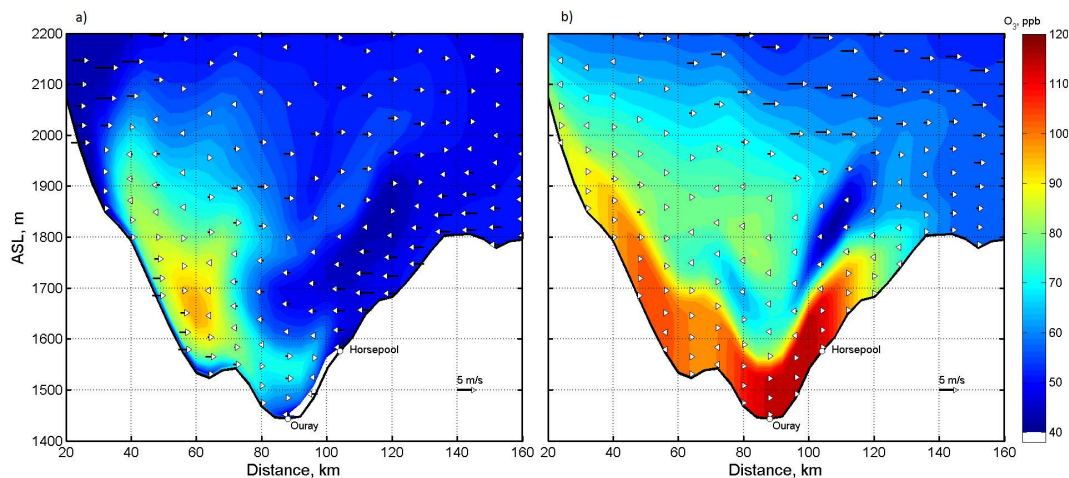


Figure 5. Simulated O₃ distribution and horizontal wind vectors (west to east direction in the WRF grid) over the UB. The surface stations Horse Pool and Ouray along the cross section are shown; **(a)** early morning (05:00 MST), **(b)** afternoon (15:00 MST) on 5 February 2013.

Title Page

Abstract

Introduction

Conclusions

References

Tables

Figures

◀

▶

◀

▶

Back

Close

Full Screen / Esc

Printer-friendly Version

Interactive Discussion

Understanding high wintertime ozone pollution events in an oil and natural gas producing region

R. Ahmadov et al.

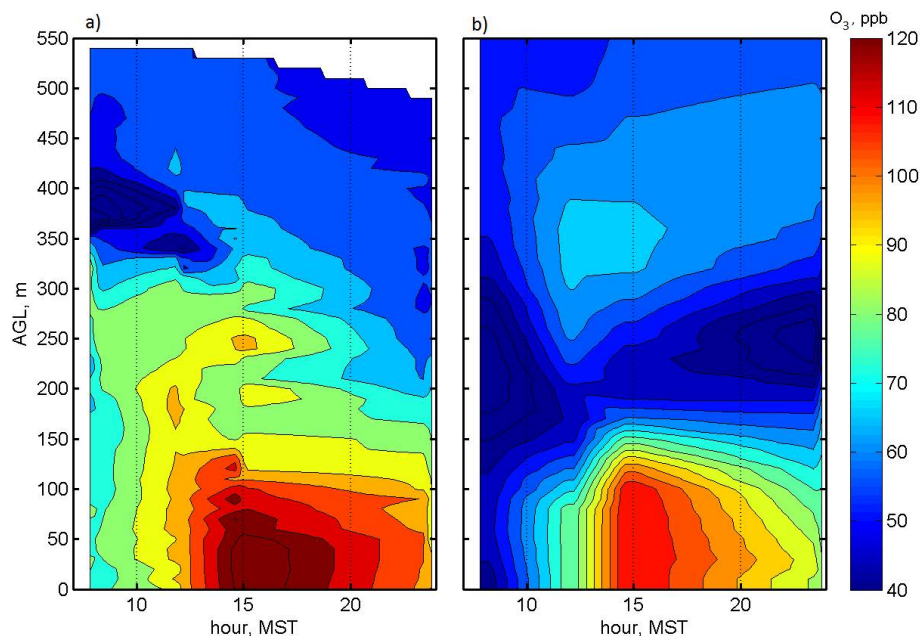


Figure 6. Vertical O_3 distribution above the Horse Pool site, 5 February 2013; **(a)** measured by the tethersonde; **(b)** modeled. There is data from 8 tethersonde profiles in **(a)**. The O_3 concentration values were interpolated for other times of the day.

[Title Page](#)[Abstract](#)[Introduction](#)[Conclusions](#)[References](#)[Tables](#)[Figures](#)[◀](#)[▶](#)[◀](#)[▶](#)[Back](#)[Close](#)[Full Screen / Esc](#)[Printer-friendly Version](#)[Interactive Discussion](#)

Understanding high wintertime ozone pollution events in an oil and natural gas producing region

R. Ahmadov et al.

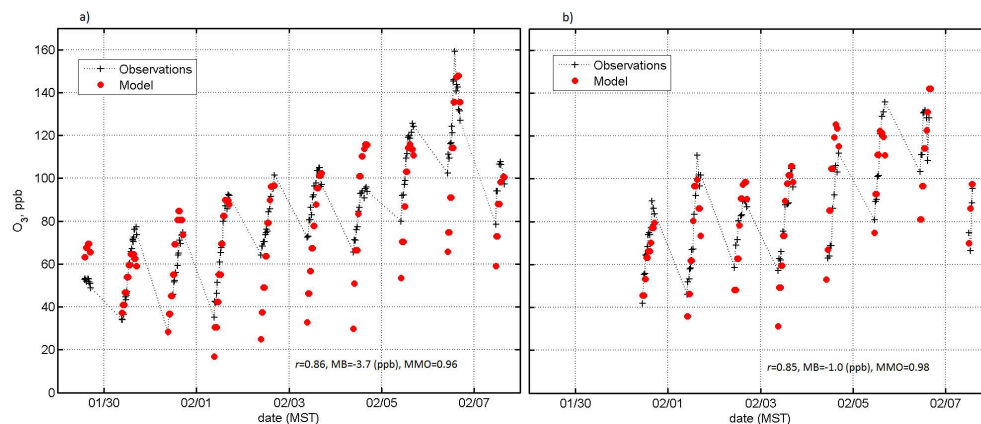


Figure 7. Time series of the daytime (09:00–17:00 MST) O₃ concentrations measured near the surface by tether sondes and modeled at (a) Oury and (b) Fantasy Canyon sites in the winter of 2013. The locations of these tether sonde launches are shown in Fig. 1. Here the modeled O₃ values are shown solely for the times when the tether sonde measurements were conducted.

Title Page

Abstract

Introduction

Conclusions

References

Tables

Figures

◀

▶

◀

▶

Back

Close

Full Screen / Esc

Printer-friendly Version

Interactive Discussion